Simultaneous vibrational resonance in the amplitude and phase quadratures of an optical field based on Kerr nonlinearity

Yinuo Wang, Shan Wu, Cuicui Li, Zhenglu Duan, Min Xie, and Bixuan Fan[*]

College of Physics and Communication Electronics, Jiangxi Normal University, Nanchang 330022, China

Vibrational resonance (VR) is a nonlinear phenomenon in which the system response to a weak signal can be resonantly enhanced by applying a high-frequency modulation signal with an appropriate amplitude. The majority of VR research has focused on amplifying the amplitude or intensity of the system response to a weak signal, whereas the study of the phase information of system responses in VR remains limited. Here, we investigate the VR phenomena in both amplitude and phase quadratures of an optical field in a Kerr nonlinear cavity driven by a near-resonant weak signal and a far-detuned modulation signal. Analytical and numerical results demonstrated that the resonant enhancement in the amplitude and phase quadratures of the system response to a weak signal simultaneously occurs as the amplitude of the modulation signal is varied. There is a linear relation between the amplitude and frequency of the modulation signal for achieving an optimal VR effect. Furthermore, we generalized our study to investigate the quadrature at an arbitrary phase and determined that the VR enhancement sensitively depends on the phase. Our findings not only broaden the scope of VR research by incorporating phase information but also introduce an approach for amplifying an optical field by manipulating another optical field.

I. INTRODUCTION

Resonance refers to the phenomenon by which the amplitude of a physical system at a certain frequency overwhelms that at other frequencies, which commonly occurs in nature and can be observed or applied in nearly all branches of physics, as well as in many interdisciplinary and engineering fields. Stochastic resonance (SR) is a widely studied phenomena [1–5] in which noise is utilized to amplify the response of a bistable system to a weak input signal, and the optimal amplification or the resonance occurs when the noise-induced average transition rate matches the frequency of the weak signal. SR was first proposed by Benzi *et al.* in the study of climate change as an enhancement of the response of bistable systems to weak deterministic signals [1–3]. Over time, the study of SR has extended to various related areas, such as coherence resonance [6–8], resonant activation [9–11], noise-induced stability [12–14], noise-induced pattern formation [15–17], and noise-enhanced temporal regularity [18,19].

A noteworthy analogy to SR is vibrational resonance (VR) [20–22], which occurs when a high-frequency periodic signal replaces noise in SR to amplify the response of a nonlinear system to a weak signal. VR was first numerically observed by Landa and McClintock [20], and was then theoretically [23–26] and experimentally [27–30] demonstrated in a variety of systems. The study of conventional VR has been extended to a number of variations, that is, aperiodic VR [31,32], ghost VR [33,34], nonlinear VR [35,36], entropic VR [37,38], logical VR [39,40], and vibrational antiresonance

[41]. Owing to the deterministic and controllable nature of VR, it has demonstrated significant potential in several research fields, including weak fault detection [42,43], weak signal amplification [44,45], investigating atmospheric disturbance phenomena [46], and bioinformatics [47–50].

Most of the earlier research regarding VR has focused on the enhancement of the system response to a weak signal, whereas studies regarding the phase information of the system response in the VR phenomena [41] remain limited. In Ref. [41], Sarkar and Ray theoretically studied the phase variation of the system response in the vibrational antiresonance phenomenon and demonstrated that a large phase shift was induced by varying the amplitude of a high-frequency field. To the best of our knowledge, the phase properties of the system response to a weak signal in conventional VR have not been investigated thus far. Therefore, in this study, we investigate the VR phenomena in both the amplitude and phase quadratures of an optical signal in the context of a driven single-mode optical cavity containing a Kerr medium. Owing to the self-Kerr interaction of the cavity field, the amplitude and phase quadratures are nonlinearly coupled, providing the basis for studying the VR behaviors in both quadratures. By directly separating the fast and slow motion, we derived the approximate analytical expressions of the response amplitudes for both quadratures. The response amplitude is a typical quantity that can be used to characterize the VR phenomena, which measures the amplitude of the system response at the frequency of the weak signal to be amplified. The results demonstrated that VR simultaneously occurred in the amplitude and phase quadratures as we varied the amplitude of the modulation signal. We also performed numerical simulations to verify the analytical results and demonstrated the system
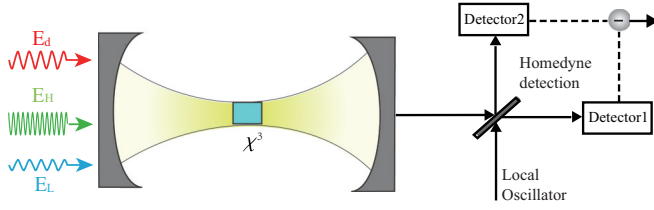
FIG. 1. Sketch of our model. A single-model optical cavity containing a third-order nonlinear Kerr medium is driven by a driving field E_d and two signal fields, E_H and E_L. E_L is a weak signal to be amplified and E_H is a modulation signal which is far detuned from the cavity resonance frequency. The output field of the cavity is detected via homodyne detection.

dynamics. The numerical results were qualitatively consistent with the analytical results. Notably, the amplitude of the phase quadrature was highly sensitive to the amplitude of the modulation signal in a certain regime, demonstrating the potential to be applied for precision measurements. In addition, the numerical results demonstrated that there was a linear relationship between the modulation amplitude and frequency for the optimal condition of the signal amplification.

In the experiments, the quadrature information of an optical field can be obtained using the standard homodyne detection technique. By adjusting the phase of the local oscillator in the homodyne detection process, the information for the desired quadrature of the system output signal can be acquired. For example, the information of the amplitude and phase quadratures discussed above can be obtained by selecting a phase of zero and $\pi/2$, respectively. To clarify the function of the phase in VR, we numerically investigated the dependence of the response amplitude on the phase of the local oscillator, and the results demonstrated that the response amplitude experienced sine-like oscillations and its maximal value did not correspond to zero or $\pi/2$. Our findings encourage further investigation of the interplay between VR and the optical phase information, and provide theoretical guidance for simultaneously amplifying the amplitude and phase quadratures of system responses to a weak optical field by applying another optical field. This may have potential for applications in optical signal detection and energy transfers between optical fields with different frequencies.

In Sec. II, we introduce the physical model and provide the theoretical formulation. The main results are presented in Sec. III, including the VR phenomena in the amplitude and phase quadratures of the system response, and the dependence of VR behaviors on the system parameters. Finally, Sec. IV concludes our study.

II. MODEL AND THEORETICAL ANALYSES

As shown in Fig. 1, the model being considered is an anharmonic optical oscillator with a self-Kerr interaction, that is, a single-mode optical cavity containing a nonlinear Kerr medium. The cavity mode is driven by three fields with different frequencies, one driving field (E_d) and two signal fields (E_L and E_H). The Hamiltonian describing the system rotating at the frequency of the driving field is given

($\hbar = 1$) as

$$\hat{H} = \Delta\hat{a}^\dagger\hat{a} + \chi(\hat{a}^\dagger\hat{a})^2 + iE_d(\hat{a}^\dagger - \hat{a})$$
$$+ iE_L(e^{-i\Delta_L t}\hat{a}^\dagger - e^{i\Delta_L t}\hat{a}) + iE_H(e^{-i\Delta_H t}\hat{a}^\dagger - e^{i\Delta_H t}\hat{a}),$$
$$(1)$$

where the cavity mode with the resonance frequency ω_c is represented by the annihilation operator $\hat{a}$. The detunings are defined as $\Delta = \omega_c - \omega_d$, $\Delta_L = \omega_L - \omega_d$, and $\Delta_H = \omega_H - \omega_d$. χ is the third-order nonlinear coefficient of the Kerr medium. To satisfy the condition of VR, we assume that the two signals have distinguishing frequencies, that is, $\Delta_H \gg \Delta_L$.

Under the condition of a weak nonlinearity and strong driving field and with the inclusion of the dissipation induced by the interaction with the environment, we can approximately derive the equation of motion for the mean amplitude of the cavity field $\alpha = \langle\hat{a}\rangle$:

$$\frac{d\alpha}{dt} = -(i(\Delta + \chi) + \kappa/2)\alpha - 2i\chi|\alpha|^2\alpha + E_d$$
$$+ E_L e^{-i\Delta_L t} + E_H e^{-i\Delta_H t}. \qquad (2)$$

Here, we have approximately factorized the correlation terms, e.g., $\langle\hat{a}^\dagger\hat{a}^2\rangle \approx \langle\hat{a}^\dagger\rangle\langle\hat{a}\rangle^2$. Note, α is a complex variable and therefore Eq. (2) is different from the typical equation of motion in classical nonlinear systems used for investigating the VR phenomena. To transform Eq. (2) into real variables, we defined the amplitude quadrature $x = \frac{\alpha + \alpha^*}{2}$ and phase quadrature $y = \frac{\alpha - \alpha^*}{2i}$, thus the equations of motion of the system can be expressed as follows:

$$\frac{dx}{dt} = -\frac{\kappa}{2}x + (\Delta + \chi)y + 2\chi(x^2 + y^2)y$$
$$+ E_d + E_L\cos\Delta_L t + E_H\cos\Delta_H t, \qquad (3)$$

$$\frac{dy}{dt} = -\frac{\kappa}{2}y - (\Delta + \chi)x - 2\chi(x^2 + y^2)x$$
$$- E_L\sin\Delta_L t - E_H\sin\Delta_H t. \qquad (4)$$

Precisely solving the coupled Eqs. (3) and (4) is complex, as they are differential equations containing nonlinear terms and two driving signals with distinguishing frequencies. Therefore, the slow and fast motions were separated [28,35,41,51]. Thus, the quadrature variables x and y were rewritten as the summation of the slow and fast motions:

$$x(t) = X(t) + \Psi_x(t, \tau = \Delta_H t), \qquad (5)$$

$$y(t) = Y(t) + \Psi_y(t, \tau = \Delta_H t). \qquad (6)$$

Here, $X(t)$ and $Y(t)$ are the variables characterizing the slow-motion components of the system response caused by E_L, whereas $\Psi_x(t, \tau)$ and $\Psi_y(t, \tau)$ are variables characterizing the fast-motion components caused by E_H, which satisfy

$$\langle\Psi_x(t, \tau)\rangle = \int_0^{2\pi}\Psi_x(t, \tau)d\tau = 0, \qquad (7)$$

$$\langle\Psi_y(t, \tau)\rangle = \int_0^{2\pi}\Psi_y(t, \tau)d\tau = 0. \qquad (8)$$

By substituting Eqs. (5) and (6) into Eqs. (3) and (4) and averaging over one period of the fast motion τ, the following is obtained:

$$\frac{dX}{dt} = -\frac{\kappa}{2}X + (\Delta + \chi)Y + E_d + E_L \cos \Delta_L t$$
$$+ 2\chi\left(X^2 Y + 2X\langle\Psi_x\Psi_y\rangle + Y^3 + Y\langle\Psi_x^2\rangle \right.$$
$$\left. + 3Y\langle\Psi_y^2\rangle + \langle\Psi_x^2\Psi_y\rangle + \langle\Psi_y^3\rangle\right), \qquad (9)$$

$$\frac{dY}{dt} = -\frac{\kappa}{2}Y - (\Delta + \chi)X - E_L \sin \Delta_L t$$
$$- 2\chi\left(X^3 + XY^2 + 3X\langle\Psi_x^2\rangle + X\langle\Psi_y^2\rangle \right.$$
$$\left. + 2Y\langle\Psi_x\Psi_y\rangle + \langle\Psi_x\Psi_y^2\rangle + \langle\Psi_x^3\rangle\right). \qquad (10)$$

Subsequently, the equations for the fast motion can be obtained by subtracting the slow-motion Eqs. (9) and (10) from the original-motion Eqs. (3) and (4) as follows:

$$\frac{d\Psi_x}{dt} = -\frac{\kappa}{2}\Psi_x + (\Delta + \chi)\Psi_y + E_H \cos \Delta_H t$$
$$+ 2\chi\left(X^2\Psi_y + 2XY\Psi_x + 3Y^2\Psi_y \right.$$
$$+ 2X(\Psi_x\Psi_y - \langle\Psi_x\Psi_y\rangle) + Y\left(\Psi_x^2 - \langle\Psi_x^2\rangle\right)$$
$$\left. + 3Y\left(\Psi_y^2 - \langle\Psi_y^2\rangle\right) + \Psi_x^2\Psi_y - \langle\Psi_x^2\Psi_y\rangle + \Psi_y^3 - \langle\Psi_y^3\rangle\right)$$
$$(11)$$

$$\frac{d\Psi_y}{dt} = -\frac{\kappa}{2}\Psi_y - (\Delta + \chi)\Psi_x - E_H \sin \Delta_H t$$
$$- 2\chi\left(3X^2\Psi_x + 2X\left(\Psi_x^2 - \langle\Psi_x^2\rangle\right) \right.$$
$$+ Y^2\Psi_x + 2XY\Psi_y + X\left(\Psi_y^2 - \langle\Psi_y^2\rangle\right)$$
$$\left. + 2Y\Psi_x\Psi_y - 2Y\langle\Psi_x\Psi_y\rangle + \Psi_x\Psi_y^2 - \langle\Psi_x\Psi_y^2\rangle\right). \quad (12)$$

As Δ_H is assumed to be large, $\dot{\Psi}_x, \dot{\Psi}_y \gg \Psi_x, \Psi_y$, we can obtain the approximate solutions for the fast-motion variables as follows:

$$\Psi_x \approx \frac{E_H}{\Delta_H} \sin \Delta_H t, \qquad (13)$$

$$\Psi_y \approx \frac{E_H}{\Delta_H} \cos \Delta_H t. \qquad (14)$$

We then obtain $\langle\Psi_x^2\rangle = \langle\Psi_y^2\rangle = \frac{E_H^2}{2\Delta_H^2}$ and $\langle\Psi_x\Psi_y\rangle = \langle\Psi_x^2\Psi_y\rangle = \langle\Psi_x\Psi_y^2\rangle = 0$. By substituting these approximate solutions for the fast motion into the equations of motion for the slow motion [Eqs. (9) and (10)], we can obtain the approximate equations merely for the slow motion of the system variables, that is,

$$\frac{dX}{dt} = -\frac{\kappa}{2}X + \left(\Delta + \chi + \frac{4\chi E_H^2}{\Delta_H^2}\right)Y$$
$$+ 2\chi(X^2 Y + Y^3) + E_d + E_L \cos \Delta_L t, \qquad (15)$$

$$\frac{dY}{dt} = -\frac{\kappa}{2}Y - \left(\Delta + \chi + \frac{4\chi E_H^2}{\Delta_H^2}\right)X$$
$$- 2\chi(X^3 + XY^2) - E_L \sin \Delta_L t. \qquad (16)$$

Equations (15) and (16) demonstrate that the high-frequency signal impacts the steady-state properties of the system by the additional detuning applied to the cavity field.

To evaluate the system response to the weak signal E_L, we first searched for the steady-state solution for X and Y in the absence of the weak signal. The steady-state solution of the field intensity $|\alpha|_s^2$ simply satisfies the following equation:

$$4\chi^2\left(|\alpha|_s^2\right)^3 + 4\chi\left(\Delta + \chi + 4\chi E_H^2/\Delta_H^2\right)\left(|\alpha|_s^2\right)^2$$
$$+ [(\Delta + \chi)^2 + \kappa^2/4]|\alpha|_s^2 - E_d^2 = 0, \qquad (17)$$

which is a cubic equation of $|\alpha|_s^2$ and can be solved by a standard formula or numerically. From Eqs. (15) and (16) and the relationship of $|\alpha|_s^2 = X_s^2 + Y_s^2$, we can obtain the steady-state solution of the field quadratures as follows:

$$Y_s = -\frac{2}{\kappa}\left(\Delta + \chi + 2\chi|\alpha|_s^2\right), \qquad (18)$$

$$X_s = \frac{E_d}{\kappa/2 - Y_s\left(\Delta + \chi + 2\chi|\alpha|_s^2\right)}. \qquad (19)$$

Subsequently, we studied the deviation of X and Y from the steady-state solution when a weak signal was applied. Therefore, we expressed X and Y as the summation of their stable solutions and small deviation parts owing to the signal incidence as follows:

$$X = X_s + \delta X, \qquad (20)$$

$$Y = Y_s + \delta Y. \qquad (21)$$

Here, $(\delta X, \delta Y)$ are the deviations of the system responses (X, Y) from one set of the steady-state solution (X_s, Y_s).

As the δX and δY deviations were assumed to be small, the nonlinear terms were ignored and the linear equations of motion were obtained for $(\delta X, \delta Y)$:

$$\frac{d\delta X}{dt} = M_{11}\delta X + M_{12}\delta Y + E_L \cos \Delta_L t, \qquad (22)$$

$$\frac{d\delta Y}{dt} = M_{22}\delta Y + M_{21}\delta X - E_L \sin \Delta_L t, \qquad (23)$$

where $M_{11} = 4\chi X_s Y_s - \frac{\kappa}{2}$, $M_{12} = \Delta + \chi + \frac{4\chi E_H^2}{\Delta_H^2} + 2\chi X_s^2 + 6\chi Y_s^2$, $M_{21} = -(\Delta + \chi + \frac{4\chi E_H^2}{\Delta_H^2} + 6\chi X_s^2 + 2\chi Y_s^2)$, and $M_{22} = -(4\chi X_s Y_s + \frac{\kappa}{2})$. The solutions can be obtained by certain mathematical derivations:

$$\delta X = A \cos(\Delta_L t) + B \sin(\Delta_L t), \qquad (24)$$

$$\delta Y = C \cos(\Delta_L t) + D \sin(\Delta_L t). \qquad (25)$$

Here, the coefficients are defined as follows:

$$A = \frac{E_L}{C_3}[\Delta_L C_2 M_{22} M_{12}$$
$$+ \Delta_L(\Delta_L M_{12} + C_1)(C_1 M_{11} - M_{21} M_{22} M_{12})], \quad (26)$$

$$B = \frac{1}{C_2}[A(M_{11}C_1 - M_{21}M_{22}M_{12}) + E_L(\Delta_L M_{12} + C_1)], \quad (27)$$

$$C = -\frac{1}{C_1}[AM_{21}M_{22} + \Delta_L(BM_{21} - E_L)], \qquad (28)$$

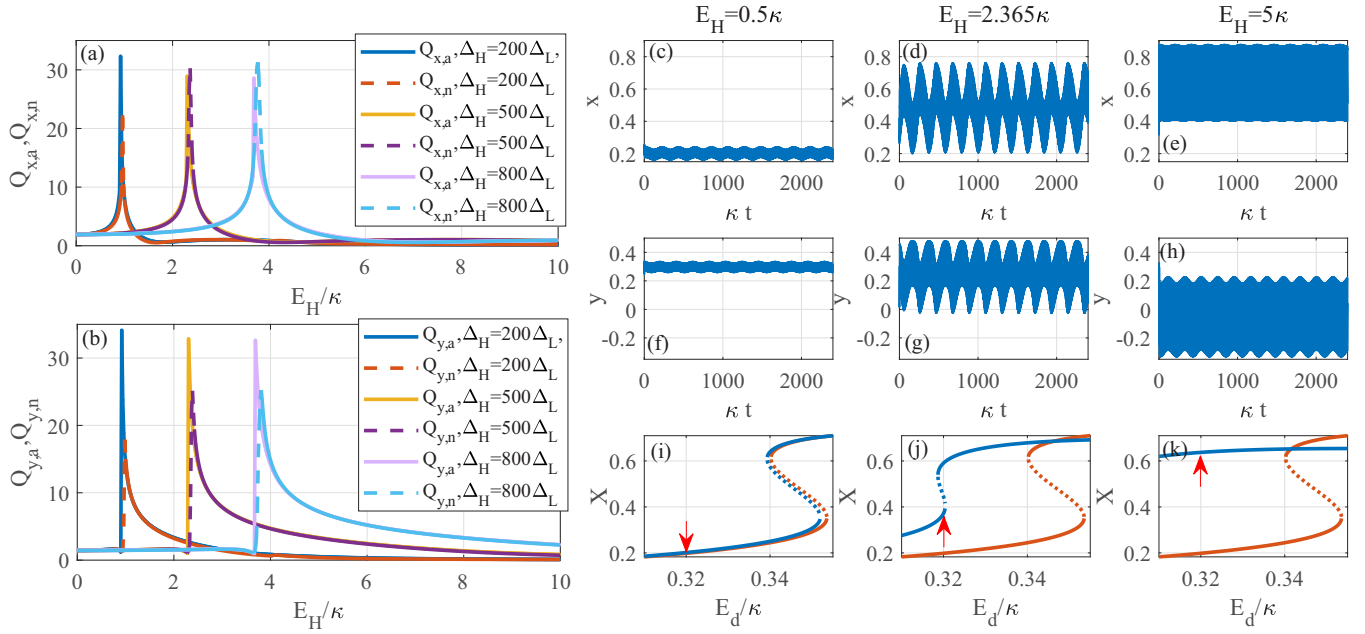$$D = \frac{AM_{21} + CM_{22}}{\Delta_L}, \qquad (29)$$

FIG. 2. The VR phenomena in both the amplitude and phase quadratures of a weak optical signal by varying the amplitude of the modulation signal E_H. (a) and (b) Comparison of the analytical and numerical results for the response amplitudes in two quadratures as E_H is varied at three modulation frequencies ($\Delta_H = 200\Delta_L$, $500\Delta_L$, and $800\Delta_L$). The solid curves represent the analytical results $Q_{x,a}$ and $Q_{y,a}$, whereas the dashed curves represent the numerical results $Q_{x,n}$ and $Q_{y,n}$. (c)–(e) Time evolution of the amplitude quadrature of the cavity field for $E_H = 0.5\kappa$, 2.365κ, 5κ. (f)–(h) Time evolution of the phase quadrature corresponding to (c)–(e). (i)–(k) Stability curves: Steady-state solution of X as a function of the driving amplitude E_d. As labeled by the red arrow, $E_d = 0.32\kappa$ was selected for (a)–(h). The other parameters were as follows: $\Delta = -2\kappa$, $\chi = \kappa$, $E_L = 0.004\kappa$, and $\Delta_L = 0.03\kappa$.

with $C_1 = \Delta_L^2 + M_{22}^2$, $C_2 = \Delta_L(M_{21}M_{12} + C_1)$, and $C_3 = C_2 M_{21} M_{22}^2 M_{12} - C_1 C_2(\Delta_L^2 + M_{21}M_{12}) - \Delta_L(M_{11}C_1 - M_{21}M_{22}M_{12})(C_1 M_{11} - M_{21}M_{22}M_{12})$.

A standard measure of quantitatively characterizing the VR phenomena is the response amplitude Q, which is defined as the ratio between the amplitude of the system response at the signal frequency and amplitude of the input signal. As both quadratures of the cavity field are involved in our model, we evaluated the response amplitudes for the amplitude and phase quadratures as follows:

$$Q_{x,a} = \frac{\sqrt{A^2 + B^2}}{E_L}, \tag{30}$$

$$Q_{y,a} = \frac{\sqrt{C^2 + D^2}}{E_L}. \tag{31}$$

These approximate analytical expressions [Eqs. (30) and (31)] are the basic results obtained for analyzing the VR behavior in our system.

III. RESULTS AND DISCUSSION

Based on the analytical expressions [Eqs. (30) and (31)], we presented the response amplitudes $Q_{x,a}$ and $Q_{y,a}$ as a function of the modulation amplitude E_H for three different modulation frequencies of $\Delta_H = 200\Delta_L$, $500\Delta_L$, $800\Delta_L$ [solid curves in Figs. 2(a) and 2(b)]. All the response amplitudes $Q_{x,a}$ and $Q_{y,a}$ apparently peak at certain values of E_H, indicating the occurrence of VR. As the modulation frequency

Δ_H increased, the peak positions of $Q_{x,a}$ and $Q_{y,a}$ tended to shift to larger values of E_H, which is consistent with the results obtained in Refs. [35,52]. This can be explained by Eqs. (15) and (16), which indicate that the value of E_H^2/Δ_H^2 must be maintained above a certain level to ensure that the high-frequency signal has an effective influence on the system. In addition, the peak positions of $Q_{x,a}$ and $Q_{y,a}$ are nearly overlapping in the axis of E_H with the same modulation frequency Δ_H, which implies that VR simultaneously occurs in two quadratures of the system response. Note that the $Q_{y,a}$ curves exhibit a sharp transition, which reveals the high sensitivity of $Q_{y,a}$ to the variation of the controlling parameter E_H.

To verify the validity of the aforementioned approximated analytical results, the equation of motion for α [Eq. (2)] was numerically solved using the fourth-order Runge-Kutta method, and the Fourier components of the amplitude and phase quadratures at the characteristic frequency of the weak signal (Δ_L) were computed as follows:

$$Q_{x,s} = \frac{2}{n\pi} \int_0^{nT} dt\, x(t)\sin(\Delta_L t), \tag{32}$$

$$Q_{x,c} = \frac{2}{n\pi} \int_0^{nT} dt\, x(t)\cos(\Delta_L t), \tag{33}$$

$$Q_{y,s} = \frac{2}{n\pi} \int_0^{nT} dt\, y(t)\sin(\Delta_L t), \tag{34}$$

$$Q_{y,c} = \frac{2}{n\pi} \int_0^{nT} dt\, y(t)\cos(\Delta_L t), \tag{35}$$

where $T = 2\pi/\Delta_L$ is the period of the weak signal E_L, n is the number of periods of the slow motion determined by the weak signal in the simulation, and $Q_{j,s}(j = x, y)$ and $Q_{j,c}(j = x, y)$ represent the sine and cosine components for amplitude and phase quadratures, respectively. Subsequently, the numerical response amplitudes for the two quadratures can be obtained as follows:

$$Q_{x,n} = \frac{\sqrt{Q_{x,s}^2 + Q_{x,c}^2}}{E_L} \tag{36}$$

$$Q_{y,n} = \frac{\sqrt{Q_{y,s}^2 + Q_{y,c}^2}}{E_L}. \tag{37}$$

The value of $Q_{j,n}$ $(j = x, y)$ is proportional to the Fourier transform coefficient at $\omega = \Delta_L$, that is, $F_x(\omega) = \int_0^{+\infty} x(t)e^{i\omega t}dt$ or $F_y(\omega) = \int_0^{+\infty} y(t)e^{i\omega t}dt$. The numerical results, $Q_{x,n}$ and $Q_{y,n}$, are indicated by the dashed curves in Fig. 2(a) By comparison, the numerical results were apparently qualitatively consistent with the analytical results, demonstrating the validity of the analytical calculations; however, there were certain deviations between the two.

To understand the physical reasons behind the trends of $Q_{x,n}$ and $Q_{y,n}$ as E_H was varied, Figs. 2(c)–2(h) present the dynamics of the amplitude and phase quadratures at the three representative points of $E_H = 0.5\kappa, 2.365\kappa, 5\kappa$, as well as the corresponding stability curves. For simplicity, $\Delta_H = 500\Delta_L$ was considered as an example. When $E_H = 0.5\kappa$, the modulation signal was weak and the system was in the monostable state, as shown in Fig. 2(i). Thus, the signals in both quadratures oscillated around the steady-state value with a small amplitude [Figs. 2(d) and 2(g)], and the amplification of the weak signal was not significant. When E_H was increased to 2.365κ, which is the optimal value for maximizing $Q_{x,n}$ and $Q_{y,n}$ [Figs. 2(a) and 2(b)], the system became bistable [Fig. 2(j)], and the system responses in both quadratures experienced oscillations with notably larger amplitudes [Figs. 2(c) and 2(f)], resulting in significantly amplified signals at the frequency of Δ_L. When the amplitude of the high-frequency signal was further increased, that is, $E_H = 5\kappa$, the system became monostable once again [Fig. 2(k)] and the low-frequency motion was nearly buried in the strong rapid oscillations [Figs. 2(e) and 2(h)], which is consistent with the low $Q_{x,n}$ and $Q_{y,n}$ presented in Figs. 2(a) and 2(b).

In order to more deeply explore the mechanism of VR in our system, we use MATCONT [53,54] to perform bifurcation analysis on our system. Based on the equations of slow motion [Eqs. (15) and (16)] with including the influence of E_H and excluding the weak signal, the equilibrium curve $X - E_H$ is plotted in Fig. 3. It is seen that in the range of $E_H \in (2.29\kappa, 2.39\kappa)$ there exist two limit points (LPs) on the equilibrium curve, indicating the occurrence of limit point bifurcation. By comparing this equilibrium curve with the resonance curve ($Q_x - E_H$) in Fig. 3(a), we can observe that the parameter ranges of these two curves nearly perfectly overlap. It implies that the occurrence of VR is closely related to the appearance of LP bifurcation. In fact, earlier literatures [55,56] discussed the relation between VR and bifurcations. To further investigate the detailed dependence of the system
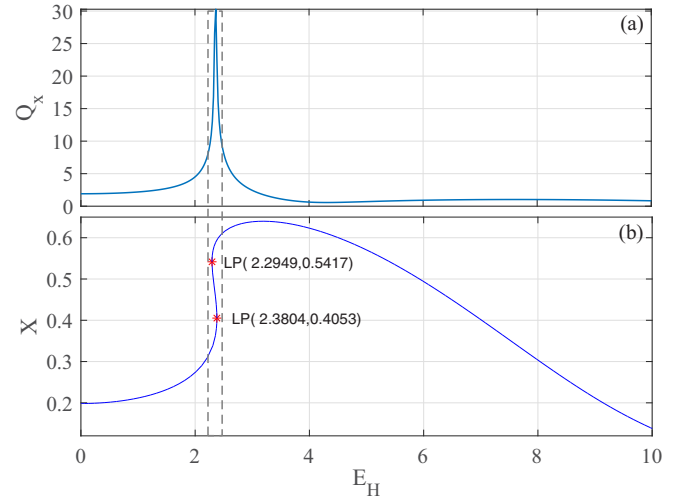

FIG. 3. (a) Q_x as a function of E_H for $\Delta_H = 500\Delta_L$. [This curve is the same as the brown dashed curve in Fig. 2(a) and it is plotted here for comparison with (b).] (b) The steady-state value of X as a function of E_H based on Eqs. (15) and (16) with $E_L = 0$ (obtained using MATCONT). LP presents the limit point. The other parameters are the same as those in Fig. 2.

responses on the properties of the modulation signal, the response amplitudes of the two quadratures were plotted in the $E_H - \Delta_H$ plane, as shown in Figs. 4(a) and 4(b), which demonstrated an apparent linear relationship between E_H and Δ_H for achieving resonance. These results are consistent with previous analytical analyses, which demonstrated that the modulation signal modifies the properties of the system stability by the factor of E_H^2/Δ_H^2. In addition, as E_H was increased from 0 to 4κ, the system responses in the two quadratures gradually increased. However, when $E_H > 4\kappa$, the system response saturated, indicating that an extremely large E_H cannot induce a significant enhancement of the system responses and
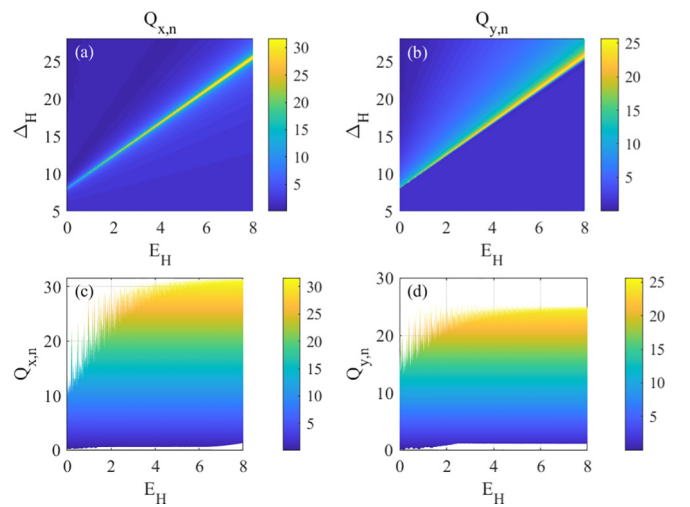

FIG. 4. Dependence of the response amplitudes $Q_{x,n}$ and $Q_{y,n}$ on the parameters of the modulation signal (E_H and Δ_H). (a) $Q_{x,n}$ in the E_H-Δ_H plane; (b) $Q_{y,n}$ in the E_H-E_L plane. (c) and (d) View of the variance of $Q_{x,n}$ and $Q_{y,n}$ vs E_H corresponding to (a) and (b). The parameters are as follows: $\Delta = -2\kappa$, $\chi = \kappa$, , $E_d = 0.32\kappa$, $E_L = 0.004\kappa$, and $\Delta_L = 0.03\kappa$.
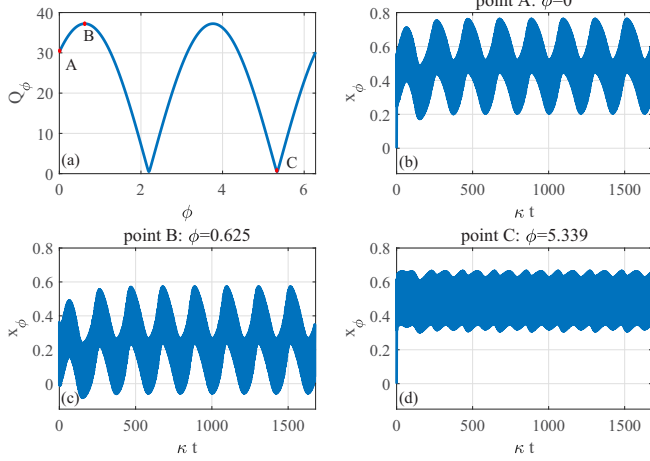
FIG. 5. (a) Response amplitude of an arbitrary quadrature x_ϕ vs the phase ϕ. (b)–(d) Time evolution of x_ϕ at three representative points including A, B, and C in (a). Here, $E_H = 2.365\kappa$, $\Delta_H = 500\Delta_L$, and the other parameters are the same as those shown in Fig. 3.

a moderate modulation signal is adequate for achieving a good VR enhancement.

The output quadrature from homodyne detection apparently relies on the phase of the local oscillator (labeled as ϕ), that is, x and y presented in the preceding section correspond to $\phi = 0$ and $\phi = \pi/2$, respectively. To generalize our results, the enhancement of the system response at the signal frequency of Δ_L for an arbitrary phase in the homodyne detection was studied. In this case, the homodyne signal is expressed as follows:

$$x_{\phi,\text{out}} = \sqrt{\kappa_0} x_\phi = \frac{1}{2}(\alpha_{\text{out}} e^{i\phi} + \alpha_{\text{out}}^* e^{-i\phi}). \quad (38)$$

Here, α_{out} is the amplitude of the output cavity field, which is proportional to the intracavity amplitude α, that is, $\alpha_{\text{out}} = \sqrt{\kappa_0}\alpha$ ($\sqrt{\kappa_0}$ is the coupling coefficient between the cavity and the homodyne detection device). Thus, we defined the response amplitudes for the quadrature of the phase ϕ as follows:

$$Q_\phi = \frac{\sqrt{Q_{\phi,s}^2 + Q_{\phi,c}^2}}{E_L}, \quad (39)$$

where the sine and cosine Fourier components at the phase ϕ are as follows:

$$Q_{\phi,s} = \frac{2}{n\pi} \int_0^{nT} dt \, \frac{1}{2}(\alpha e^{i\phi} + \alpha^* e^{-i\phi}) \sin(\Delta_L t), \quad (40)$$

$$Q_{\phi,c} = \frac{2}{n\pi} \int_0^{nT} dt \, \frac{1}{2}(\alpha e^{i\phi} + \alpha^* e^{-i\phi}) \cos(\Delta_L t). \quad (41)$$

As demonstrated in Fig. 5(a), the response amplitude Q_ϕ oscillated in a sine-like form as the phase varied from 0 to 2π, indicating that the system response was phase sensitive. Notably, Q_ϕ did not peak at $\phi = 0$ or $\phi = \pi/2$. Namely, selecting a proper phase of the local oscillator facilitates the signal enhancement effect in VR. To clarify the cause of variation of Q_ϕ, the time evolution x_ϕ of several representative points, including A: $\phi = 0$ (x quadrature), B: $\phi = 0.625$ (one peak of the Q_ϕ curve), and C: $\phi = 5.339$ (one dip of Q_ϕ curve), are presented in Figs. 5(b)–5(d). At the peak, the oscillation amplitude of x_ϕ is apparently larger than that of $\phi = 0$, whereas at the dip, x_ϕ oscillates at significantly high frequencies associated with a small amplitude of the slow variations, because the varying phase ϕ corresponds to the superposition of the real and imaginary parts of α with different weights. These dynamical behaviors are consistent with the values of Q_ϕ.

IV. CONCLUSION

In this study, the VR phenomenon in a Kerr nonlinear optical cavity with multiple signals was thoroughly analyzed. Contrary to the majority of prior research regarding VR, we incorporated the phase in the investigation of VR. More specifically, we analytically and numerically studied the enhancement in the amplitude and phase quadratures of the system response to a weak low-frequency optical signal by manipulating a high-frequency optical signal. We clarified the optimal parameter regimes required to achieve an effective VR effect. In addition, we generalized our study to an arbitrary quadrature of the system response and found that the system response sensitively relies on the phase of the local oscillator in the homodyne detection. Our study provides a better understanding of the VR mechanism as well as a theoretical guidance for amplifying a weak optical signal by controlling another optical field based on the Kerr nonlinearity.

[1] R. Benzi, A. Sutera, and A. Vulpiani, The mechanism of stochastic resonance, J. Phys. A: Math. Gen. **14**, L453 (1981).

[2] R. Benzi, G. Parisi, A. Sutera, and A. Vulpiani, Stochastic resonance in climatic change, Tellus **34**, 10 (1982).

[3] R. Benzi, G. Parisi, A. Sutera, and A. Vulpiani, A theory of stochastic resonance in climatic change, SIAM J. Appl. Math. **43**, 565 (1983).

[4] L. Gammaitoni, P. Hänggi, P. Jung, and F. Marchesoni, Stochastic resonance, Rev. Mod. Phys. **70**, 223 (1998).

[5] T. Wellens, V. Shatokhin, and A. Buchleitner, Stochastic resonance, Rep. Prog. Phys. **67**, 45 (2004).

[6] A. S. Pikovsky and J. Kurths, Coherence resonance in a noise-driven excitable system, Phys. Rev. Lett. **78**, 775 (1997).

[7] H. Gang, T. Ditzinger, C. Z. Ning, and H. Haken, Stochastic resonance without external periodic force, Phys. Rev. Lett. **71**, 807 (1993).

[8] O. V. Ushakov, H.-J. Wünsche, F. Henneberger, I. A. Khovanov, L. Schimansky-Geier, and M. A. Zaks, Coherence resonance near a Hopf bifurcation, Phys. Rev. Lett. **95**, 123903 (2005).

[9] C. R. Doering and J. C. Gadoua, Resonant activation over a fluctuating barrier, Phys. Rev. Lett. **69**, 2318 (1992).

[10] M. Marchi, F. Marchesoni, L. Gammaitoni, E Menichella-Saetta, and S. Santucci, Resonant activation in a bistable system, Phys. Rev. E **54**, 3479 (1996).

[11] P. K. Ghosh and D. S. Ray, A parametric variant of resonant activation: Two-state model approach, J. Chem. Phys. **125**, 124102 (2006).

[12] R. N. Mantegna and B. Spagnolo, Noise enhanced stability in an unstable system, Phys. Rev. Lett. **76**, 563 (1996).

[13] C. Zeng, C. Zhang, J. Zeng, R. Liu, and H. Wang, Noise-enhanced stability and double stochastic resonance of active Brownian motion, J. Stat. Mech. (2015) P08027.

[14] C. Guarcello, D. Valenti, A. Carollo, and B. Spagnolo, Stabilization effects of dichotomous noise on the lifetime of the superconducting state in a long Josephson junction, Entropy **17**, 2862 (2015).

[15] A. Sanz-Anchelergues, A. M. Zhabotinsky, I. R. Epstein, and A. P. Munuzuri, Turing pattern formation induced by spatially correlated noise, Phys. Rev. E **63**, 056124 (2001).

[16] G. Stegemann, A. G. Balanov, and E. Schöll, Noise-induced pattern formation in a semiconductor nanostructure, Phys. Rev. E **71**, 016221 (2005).

[17] D. Das and D. S. Ray, Dichotomous-noise-induced pattern formation in a reaction-diffusion system, Phys. Rev. E **87**, 062924 (2013).

[18] D. Yu, M. Xie, Y. Cheng, and B. Fan, Noise-induced temporal regularity and signal amplification in an optomechanical system with parametric instability, Opt. Express **26**, 32433 (2018).

[19] B. Fan, X. Wu, and Z. Duan, Enhancement of white-noise-induced temporal regularity in a linear-optical system using coherent feedback, Phys. Rev. A **107**, 023708 (2023).

[20] P. S. Landa and P. V. E. McClintock, Vibrational resonance, J. Phys. A: Math. Gen. **33**, L433 (2000).

[21] S. Jeyakumari, V. Chinnathambi, S. Rajasekar, and M. A. F. Sanjuan, Single and multiple vibrational resonance in a quintic oscillator with monostable potentials, Phys. Rev. E **80**, 046608 (2009).

[22] C. Yao, Y. Liu, and M. Zhan, Frequency-resonance-enhanced vibrational resonance in bistable systems, Phys. Rev. E **83**, 061122 (2011).

[23] M. Gitterman, Bistable oscillator driven by two periodic fields, J. Phys. A: Math. Gen. **34**, L355 (2001).

[24] A. A. Zaikin, L. López, J. P. Baltanás, J. Kurths, and M. A. F. Sanjuán, Vibrational resonance in a noise-induced structure, Phys. Rev. E **66**, 011106 (2002).

[25] I. I. Blekhman and P. S. Landa, Conjugate resonances and bifurcations in nonlinear systems under biharmonical excitation, Int. J. Non Linear Mech. **39**, 421 (2004).

[26] A. Ichiki, Y. Tadokoro, and M. Takanashi, Linear response analysis of vibrational resonance in over-damped systems, J. Phys. A: Math. Theor. **45**, 385101 (2012).

[27] V. N. Chizhevsky, E. Smeu, and G. Giacomelli, Experimental evidence of vibrational resonance in an optical system, Phys. Rev. Lett. **91**, 220602 (2003).

[28] J. P. Baltanás, L. Lopez, I. I. Blechman, P. S. Landa, A. Zaikin, J. Kurths, and M. A. F. Sanjuán, Experimental evidence, numerics, and theory of vibrational resonance in bistable systems, Phys. Rev. E **67**, 066119 (2003).

[29] V. N. Chizhevsky and G. Giacomelli, Experimental and theoretical study of vibrational resonance in a bistable system with asymmetry, Phys. Rev. E **73**, 022103 (2006).

[30] V. N. Chizhevsky, Vibrational higher-order resonances in an overdamped bistable system with biharmonic excitation, Phys. Rev. E **90**, 042924 (2014).

[31] V. N. Chizhevsky and G. Giacomelli, Vibrational resonance and the detection of aperiodic binary signals, Phys. Rev. E **77**, 051126 (2008).

[32] P. X. Jia, C. J. Wu, J. H. Yang, M. A. F. Sanjuán, and G. X. Liu, Improving the weak aperiodic signal by three kinds of vibrational resonance, Nonlinear Dyn. **91**, 2699 (2018).

[33] S. Rajamani, S. Rajasekar, and M. A. F. Sanjuán, Ghost-vibrational resonance, Commun. Nonlinear Sci. Numer. Simul. **19**, 4003 (2014).

[34] B. I. Usama, S. Morfu, and P. Marquie, Vibrational resonance and ghost-vibrational resonance occurrence in Chua's circuit models with specific nonlinearities, Chaos, Solitons Fractals **153**, 111515 (2021).

[35] S. Ghosh and D. S. Ray, Nonlinear vibrational resonance, Phys. Rev. E **88**, 042904 (2013).

[36] T. L. M. Djomo Mbong, M. S. Siewe, and C. Tchawoua, Controllable parametric excitation effect on linear and nonlinear vibrational resonances in the dynamics of a buckled beam, Comm Nonlinear Sci. Numer. Simul. **54**, 377 (2018).

[37] L. Du, R. Han, J. Jiang, and W. Guo, Entropic vibrational resonance, Phys. Rev. E **102**, 012149 (2020).

[38] J. Jiang, K. Li, W. Guo, and L. Du, Energetic and entropic vibrational resonance, Chaos, Solitons & Fractals **152**, 111400 (2021).

[39] R. Gui, Y. Wang, Y. Yao, and G. Cheng, Enhanced logical vibrational resonance in a two-well potential system, Chaos, Solitons Fractals **138**, 109952 (2020).

[40] S. Huang, J. Zhang, J. Yang, H. Liu, and M. A. F. Sanjuán, Logical vibrational resonance in a symmetric bistable system: Numerical and experimental studies, Commun. Nonlinear Sci. Numer. Simul. **119**, 107123 (2023).

[41] P. Sarkar and D. S. Ray, Vibrational antiresonance in nonlinear coupled systems, Phys. Rev. E **99**, 052221 (2019).

[42] L. Xiao, X. Zhang, S. Lu, T. Xia, and L. Xi, A novel weak-fault detection technique for rolling element bearing based on vibrational resonance, J. Sound Vib. **438**, 490 (2019).

[43] L. Xiao, R. Bajric, J. Zhao, J. Tang, and X. Zhang, An adaptive vibrational resonance method based on cascaded varying stable-state nonlinear systems and its application in rotating machine fault detection, Nonlinear Dynam. **103**, 715 (2021).

[44] A. Chowdhury, M. G. Clerc, S. Barbay, I. Robert-Philip, and R. Braive, Weak signal enhancement by nonlinear

resonance control in a forced nano-electromechanical resonator, Nat. Commun. **11**, 2400 (2020).

[45] G. Madiot, S. Barbay, and R. Braive, Vibrational resonance amplification in a thermo-optic optomechanical nanocavity, Nano Lett. **21**, 8311 (2021).

[46] A. Jeevarekha and P. Philominathan, A nonlinear approach to analyse the development of tropical disturbances, Pramana **86**, 1031 (2016).

[47] B. Deng, J. Wang, X. Wei, K. M. Tsang, and W. L. Chan, Vibrational resonance in neuron populations, Chaos **20**, 013113 (2010).

[48] C. Wang, K. Yang, and S. Qu, Vibrational resonance in a discrete neuronal model with time delay, Int. J. Mod. Phys. B **28**, 1450103 (2014).

[49] M. Ge, L. Lu, Y. Xu, R. Mamatimin, Q. Pei, and Y. Jia, Vibrational mono-/bi-resonance and wave propagation in fitzhugh–nagumo neural systems under electromagnetic induction, Chaos, Solitons Fractals **133**, 109645 (2020).

[50] P. Fu, C.-J. Wang, K.-L. Yang, X.-B. Li, and B. Yu, Reentrance-like vibrational resonance in a fractional-order birhythmic biological system, Chaos, Solitons Fractals **155**, 111649 (2022).

[51] C. Jeevarathinam, S. Rajasekar, and M. A. F. Sanjuán, Theory and numerics of vibrational resonance in duffing oscillators with time-delayed feedback, Phys. Rev. E **83**, 066205 (2011).

[52] S. Roy, D. Das, and D. Banerjee, Vibrational resonance in a bistable van der Pol-Mathieu-Duffing oscillator, Int. J. Non-Linear Mech. **135**, 103771 (2021).

[53] W. Govaerts, A. Dhooge, and Y. A. Kuznetsov, MATCONT: A MATLAB package for numerical bifurcation analysis of ODEs, ACM Trans. Math. Softw. **29**, 141 (2003).

[54] Y. A. Kuznetsov, H. G. E. Meijer, A. Dhooge, W. Govaerts, and B. Sautois, New features of the software MATCONT for bifurcation analysis of dynamical systems, Math. Comput. Modell. Dynam. Syst. **14**, 147 (2008).

[55] T. O. Roy-Layinde, J. A. Laoye, O. O. Popoola, U. E. Vincent, and P. V. E. McClintock, Vibrational resonance in an inhomogeneous medium with periodic dissipation, Phys. Rev. E **96**, 032209 (2017).

[56] T. O. Roy-Layinde, J. A. Laoye, O. O. Popoola, and U. E. Vincent, Analysis of vibrational resonance in bi-harmonically driven plasma, Chaos **26**, 093117 (2016).